

Compact seaweed growth of peritectic phase on confined, flat properitectic dendrites



A. Ludwig, J. Mogeritsch

Montanuniversitaet Leoben, Department of Metallurgy, Chair for Simulation and Modelling of Metallurgical Processes, 8700 Leoben, Austria

ARTICLE INFO

Communicated by T.F. Kuech

Keywords:

Peritectic solidification
Dendritic-cellular transition
Seaweed growth

ABSTRACT

Peritectic alloys form a variety of different solidification morphologies at low growth rates. An alloy with a concentration that corresponds to the hyper-peritectic limit should show a cellular/dendritic solidification of the peritectic phase for growth velocities above the corresponding constitutional undercooling limit. However, due to nucleation retardation of the peritectic phase we observed growth of properitectic dendrites before cellular growth of the peritectic could be established. The transition happened via an overgrowth of dendrites with a thin layer of peritectic phase. The observations were made using a transparent, metal-like solidifying peritectic system that was solidified directionally in thin samples. In the gap between the flat dendrites and the tubing walls, the peritectic phase grew with a compact seaweed morphology, whereas in the interdendritic spacing it formed small-curved bumps. At same distance behind the tip region, more and more polycrystalline-like objects appeared at the elongated traces of the compact seaweed morphology.

1. Introduction

In peritectic systems, the properitectic α -phase reacts upon cooling with the liquid to yield the peritectic β -phase at the peritectic temperature T_p . At this distinct temperature, a liquid of concentration $c_{p,l}$ is in equilibrium with an α -phase of concentration $c_{p,\alpha}$ and a β -phase of concentration $c_{p,\beta}$. Alloys with compositions between $c_{p,\alpha}$ and $c_{p,\beta}$ are called hypo-peritectic, those with compositions between $c_{p,\beta}$ and $c_{p,l}$ are called hyper-peritectic [1]. Above the critical growth rate for constitutional undercooling of the two solid phases, both hypo- and hyper-peritectic alloys are supposed to solidify with α -cells/dendrites which are then covered with a solid layer of β -phase when the temperature along the α -cells/dendrites drops below T_p . For an alloy with a concentration of $c_{p,l}$, the so-called hyper-peritectic limit, cellular/dendritic solidification of β is expected for growth velocities above the constitutional undercooling limit.

Close or below the limit of constitutional undercooling of both solid phases, directional solidified peritectic alloys show a variety of complex microstructures. Corresponding investigations were made for Zn–Ag [2], Sn–Cd [3–6], Cu–Sn [7], Pb–Bi [8–12], Zn–Cu [13–15], Sn–Sb [16,17], Ti–Al [18,19], Fe–Ni [20–30], Ni–Al [31], YBCO [32], Nd–Fe–B [33] and the organic model system TRIS–NPG [34–41]. The microstructures found are isothermal peritectic coupled growth (PCG), cellular peritectic coupled growth, discrete bands, island bands, and oscillatory tree-like structures. It is especially the observation of this two-phase growth, either coupled or banded, which has drawn the

recent attention of researchers to this field [13,18,25,26,28,29,31,41].

The present authors have used in-situ observations of the organic non-faceted/non-faceted (nf/nf) peritectic system TRIS (Tris-(hydroxymethyl)aminomethane)-NPG (Neopentylglycol) to enlighten the dynamic of peritectic two-phase growth [37,38,41]. They found two different mechanisms for the formation of isothermal PCG, first via island banding, and second by reducing the growth velocity from above the critical value for morphological stability of both solid phases to a value below [37,38]. In [41] detailed observations on the formation of cycles of bands and (unsteady) PCG were given. For a near-peritectic composition and for pulling rates above the morphology stability limit of both solid phases an oscillatory solidification dynamic of dendritic/cellular kind occurred [34]. For pulling rates below these limits (i) a change of planar growth from one to the other solid phase, (ii) isothermal PCG, and (iii) lateral bands, which finally also turn into isothermal PCG, were observed.

In such in-situ observations the optical indistinguishability of the properitectic α - and the peritectic β -phase made the exact interpretation of the optical investigations difficult. The only alternative to distinguish the phases is on the basis of their different growth dynamics. As shown in this paper, the drastic change in the growth morphologies from dendrites to cells for the transition from properitectic to peritectic phase growth can be taken as unmistakable hint to identify the two different phases. In addition, it was found that the reported transition revealed some spectacular observation of seaweed-type growth.

E-mail address: ludwig@unileoben.ac.at (A. Ludwig).

<http://dx.doi.org/10.1016/j.jcrysgro.2016.09.045>

Received 8 July 2016; Received in revised form 19 September 2016; Accepted 20 September 2016

Available online 23 September 2016

0022-0248/© 2016 Elsevier B.V. All rights reserved.

Table 1
Phase diagram information of TRIS-NPG taken from [43].

Quantity	Symbol	Value
peritectic temperature	T_p	410.7 ± 2 K
α -solidus concentration at T_p	$c_{p,\alpha}$	0.47 ± 0.01 mol%
β -solidus (peritectic) concentration at T_p	$c_{p,\beta}$	0.515 ± 0.01 mol%
liquidus concentration at T_p	$c_{p,l}$	0.54 ± 0.01 mol%
α -liquidus slope at T_p	$m_{p,\alpha}$	-47.9 ± 0.1 K/mol%
β -liquidus slope at T_p	$m_{p,\beta}$	-31.0 ± 0.1 K/mol%
redistribution coefficient for α -phase at T_p	$k_{p,\alpha}$	0.87 ± 0.01
redistribution coefficient for β -phase at T_p	$k_{p,\beta}$	0.96 ± 0.01
liquid/solid temp. interval for α -phase at $c_{p,l}$	$\Delta T_{p,\alpha}$	3.35 ± 0.3 K
liquid/solid temp. interval for β -phase at $c_{p,l}$	$\Delta T_{p,\beta}$	1.05 ± 0.1 K

2. Experimental procedure

The two organic compounds TRIS and NPG form a peritectic phase diagram [42], where both the properitectic α and the peritectic β phases solidify with a non-faceted solid/liquid interface [36,43,44]. Therefore, in-situ observations of solidification phenomena using TRIS-NPG alloys can be used to understand solidification of peritectic metallic alloys. Phase diagram information for the TRIS-NPG system are gathered in Table 1. The two organic compounds were delivered as powder with an indicated high purity of 99.9+% for TRIS and 99% for NPG. An additional treatment process for NPG was used to reduce the water content and thus increase the purity. Alloys were prepared by mixing the powders of both organic substances and fusing them together. The tubings were filled by capillary force and finally sealed with glue [34–36,43]. All filling operations were done in an Argon-filled glove box. Details on the alloying and filling can be found in [43].

Directional solidification experiments with hyper-peritectic TRIS-NPG alloys were performed using a vertical micro Bridgman-furnace. Samples in thin rectangle glass tubings (0.1×2 mm² inner cross section with 100 μ m wall thickness) were pulled with a constant withdrawal speed, V , in a constant temperature gradient, G . The micro Bridgman-furnace was made of two brass blocks separated by a 7 mm gap and thermally isolated by ceramic covers. The temperatures of the brass parts were controlled by electrical resistant heaters. In each brass block a 0.4×2.5 mm² deepening was milled to guide the rectangle glass samples. The sample was illuminated through glass windows, which were placed in the ceramic covers at the adiabatic zone. Observation of the dynamic of the solid/liquid interface morphologies was done with a ZEISS microscope and recorded with a digital camera [43].

To start a solidification experiment the furnace was shortly opened and a sample was put into the desired position. As a sample is longer than the heated zone, only a sample segment of around 50 mm in length was molten. The pressure increase which might be caused by the expansion on heating and melting, was released by the fact that a solid material column at room temperature did not fill the tube completely. The low temperature faceted phases, which are stable at room temperature, reveal 10–20% higher densities compared with the high temperature plastic phases and so while cooling of the just filled sampled the contraction of the faceted phases opened up visible gaps and cracks. So the heated and finally molten segment can easily push the solid segments above and below aside and a pressure-free molten segment can form. Note that the results presented in this paper were gained by using newly filled samples, where the concentration can be assumed to be uniform along the sample length.

After the positioning, the sample was held in rest for 60 min to establish a thermal equilibrated state. During this time the solid/liquid interface in the adiabatic zone became microscopically and macroscopically planar. Afterwards, the sample was pulled with a constant pulling rate, V , through a temperature gradient, G , for up to 16 h. In a series of experimental runs, we have varied the alloy concentration from $c_0 = 0.47$ mol% to $c_0 = 0.54$ mol% and the pulling rate from

$V = 0.13$ μ m/s to $V = 0.32$ μ m/s. The temperature gradient was estimated to be $G = 6.65$ K/mm.

In this paper, the development of the solid/liquid interface morphology for a TRIS-NPG alloy with a nominal concentration of $c_0 = 0.54$ mol% is reported. Note that this concentration corresponds to the hyper-peritectic limit (see Table 1).

3. Results and discussion

The characteristic of the experiment described above is that for the samples with hyper-peritectic concentration, the interface morphology revealed a dendritic pattern for several hours and then, within minutes, changed into a cellular one, which then lasted for the remaining hours of the experiment. Fig. 1(a) gives an example of the dendritic and Fig. 1(b) of the cellular morphology. Fig. 2 shows that the transition happened due to an overgrowth of the dendrites with a second phase, which then continued to grow as cells. The observations described here were made several times with different samples having a concentration of $c_{p,l}$.

The dendrites shown in Fig. 1(a) belong to two different grains. Left from the grain boundary the dendrites are inclined anticlockwise with respect the pulling direction by $32.8 \pm 0.9^\circ$ and right from the boundary clockwise by $5.8 \pm 0.2^\circ$. The primary dendrite arm spacing for the left grain was estimated to be $\lambda_1 = 278 \pm 15$ μ m and $\lambda_1 = 264 \pm 59$ μ m for the right one. For the dendrite tip radius we have measured up $R = 13.8 \pm 1.7$ μ m and $R = 17.4 \pm 1.8$ μ m correspondingly, which is much smaller than the 100 μ m sample spacing. Therefore, a rotationally symmetrical tip shape for the tips shown in Fig. 1 might be a good approximation. Note further that the envelope of the dendrite tips is curved and the leftmost dendrite tip is slightly lagging behind. As discussed in [40] there are evidences that under the present conditions the isotherms are strictly horizontal but that due to a weak natural convection we get a small NPG enrichment at the edges, in the present case only on the left hand side. This slight NPG enrichment at the left edge of the sample defined also the position where the second phase finally nucleated. With $D = 1.3 \pm 0.3 \cdot 10^{-11}$ m²/s for the diffusion coefficient of NPG in the TRIS-NPG melt [43], we got $P_c^{\text{dendr.}} = RV/2D = 0.21$ for the solutal Péclet-number of the dendrites that grew on the right hand side of the grain boundary, for which we assume that they grew into the initial c_0 -melt.

For the cellular array shown in Fig. 1(b) we have estimated only one average primary arm spacing of $\lambda_1 = 169 \pm 38$ μ m. For the cell tip radius we got $R = 28.0 \pm 4.2$ μ m from which a solutal Péclet-number of $P_c^{\text{cells}} = 0.35$ was calculated. Note that the envelope of the cell tips is also curved with lower tips on the left hand side. However, the curving is smaller compared to the dendritic case shown in Fig. 1(a).

Not of significance for the present paper but still nice to observe is the fact that in Fig. 1(a) the coagulation of the inclined dendrites deep in the interdendritic mush formed regularly left-behind liquid pockets (like string of pearls).

As both high temperature solid phases of the peritectic TRIS-NPG system are equally transparent, they can only be identified by their different growth behavior. Note that thermodynamically for $c_0 = 0.54$ mol%, both solid phases, the properitectic α - and peritectic β -phase, are allowed to form (see Table 1). However, the chosen experimental conditions have obviously favored the growth of one solid phase before the second one appeared and finally took over the growth.

In order to identify the two different solid phases let us first compare the critical growth rate for constitutional undercooling, V_C . We got $V_{C,\alpha} = 0.02$ μ m/s for the α -phase and $V_{C,\beta} = 0.167$ μ m/s for the β -phase. So, the pulling speed of $V = 0.32$ μ m/s is around 16 larger for the α -phase and around 2 times for the β -phase. Keeping this in mind, we expect well developed dendrites to form for the α -phase and more cellular growth for the β -phase. This is the first hint that properitectic α -dendrites have been overgrown by the peritectic β -phase and not vice versa.

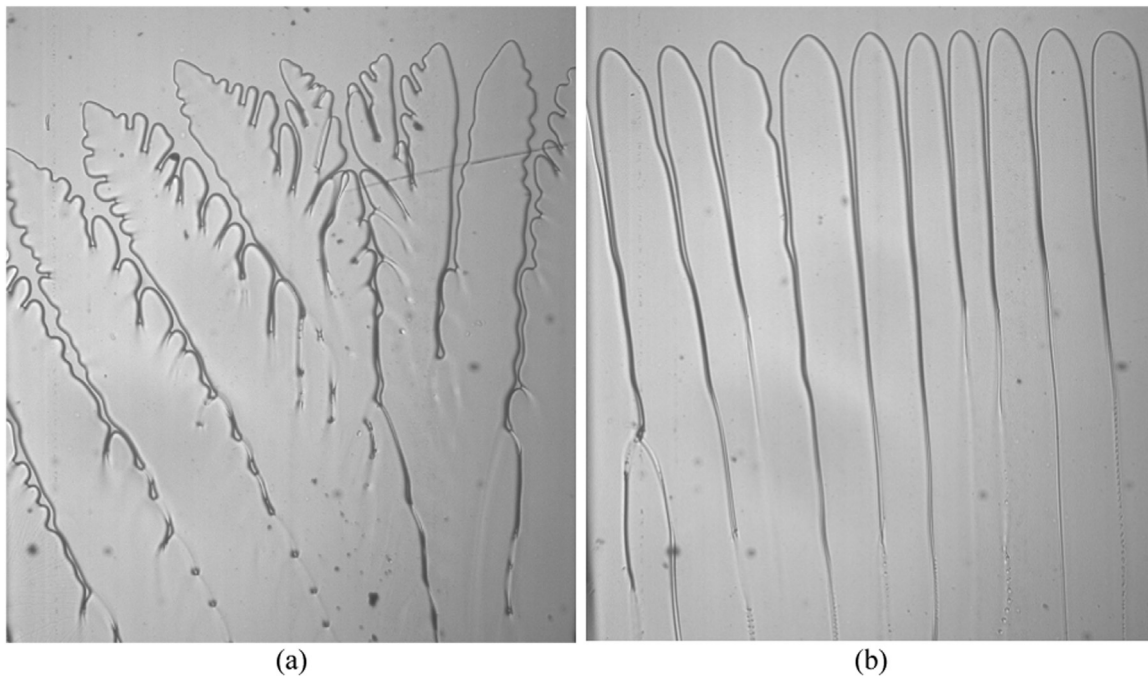


Fig. 1. (a) Dendritic growth of the TRIS-rich properitectic α phase and (b) cellular growth of the NPG-rich peritectic β phase for a TRIS-0.54 mol% NPG alloy. The width of the pictures is around 1700 μm .

The second hint can be gained by evaluating the primary arm spacing, λ_1 . If we follow the simple geometrical arguments for an approximate expression for the primary arm spacing from [45] and use¹ $\lambda_1^2 \approx 4\Delta T_0 R/G$, we get $\lambda_1^{\text{dendr.}} = 187 \mu\text{m}$ and $\lambda_1^{\text{cells}} = 133 \mu\text{m}$ for the case assuming that the α -phase has grown dendritically and β -phase as cells. The opposite assumption would lead to $\lambda_1^{\text{dendr.}} < \lambda_1^{\text{cells}}$, which is in contradiction to the observations. Although the estimated primary arm spacings are significantly smaller than the observed ones, the relative size difference reveals that Fig. 1(a) shows the growth of α -dendrites and Fig. 1(b) the growth of β -cells. Note that in [46] it is shown that when the sample thickness is smaller than λ_1 (which is definitely the case in our experiment), the observed λ_1 is significantly larger than it would be in 3D. This explains why in our case the measured spacings are larger than those predicted by theory.

In fact, both of the above arguments to identify the phases are related to the different phase diagram features of the two phases. For peritectic systems the properitectic α -phase always reveal a larger ΔT_0 and a smaller k compared to the peritectic β -phase. That is why V_C is always smaller and λ_1 is larger for the α -phase compared to the β -phase.

Let us now take a closer look on how the peritectic β -phase overgrows the properitectic α -dendrite. Fig. 2 shows three successive pictures. Fig. 3 shows a magnified view of Fig. 2(b). From these pictures the following observations can be made:

- The β -phase grew from bottom left upwards in close contact to the α -dendrite with a growth rate of around 300 $\mu\text{m/s}$ (10 times faster than the pulling speed). It can even be said that the β -phase covered, or encapsulated the α -dendrites.
- β covered the flat α -dendrite between the flat side of the dendrite and the tubing wall, but also in the interdendritic region at the secondary side arms.
- The propagating interface of the β -phase between the flat α -dendrite and the tubing wall reveals same similarity to the cauliflower structure reported in [47].
- At the upper side of inclined α -dendrites, β forms occasionally

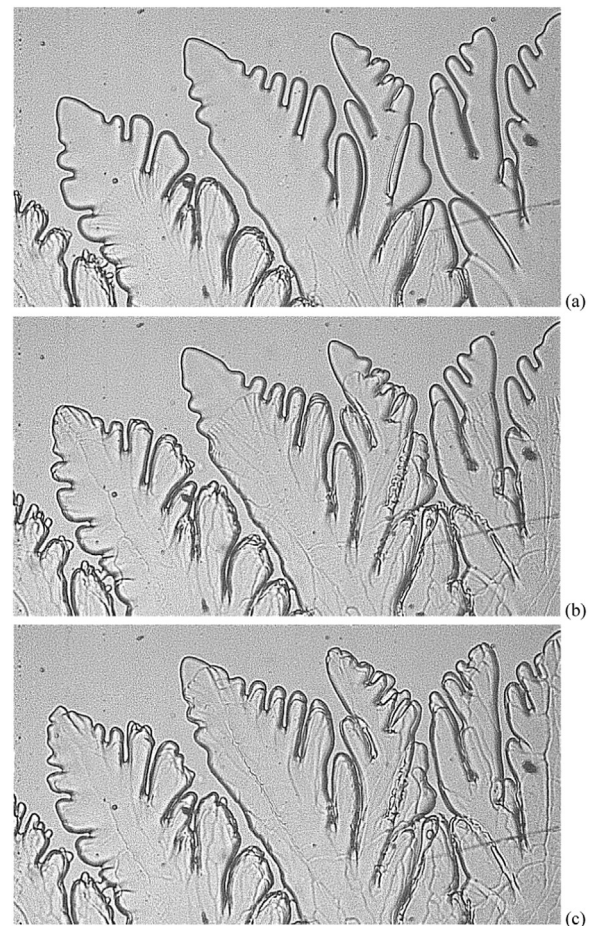


Fig. 2. Overgrowth of the properitectic α -phase dendrites with the peritectic β -phase. The β -phase growth can be seen by the weak contrasted interface which propagates from the left bottom area in (a) upwards in (b) and (c). The interval between the pictures is $\Delta t=30 \text{ s}$. The width of the pictures is around 1150 μm .

¹ Different to [45] we have considered 2D pattern rather than an hexagonal arrangement of dendrites. Thus, we got a factor of 4 rather than 3.

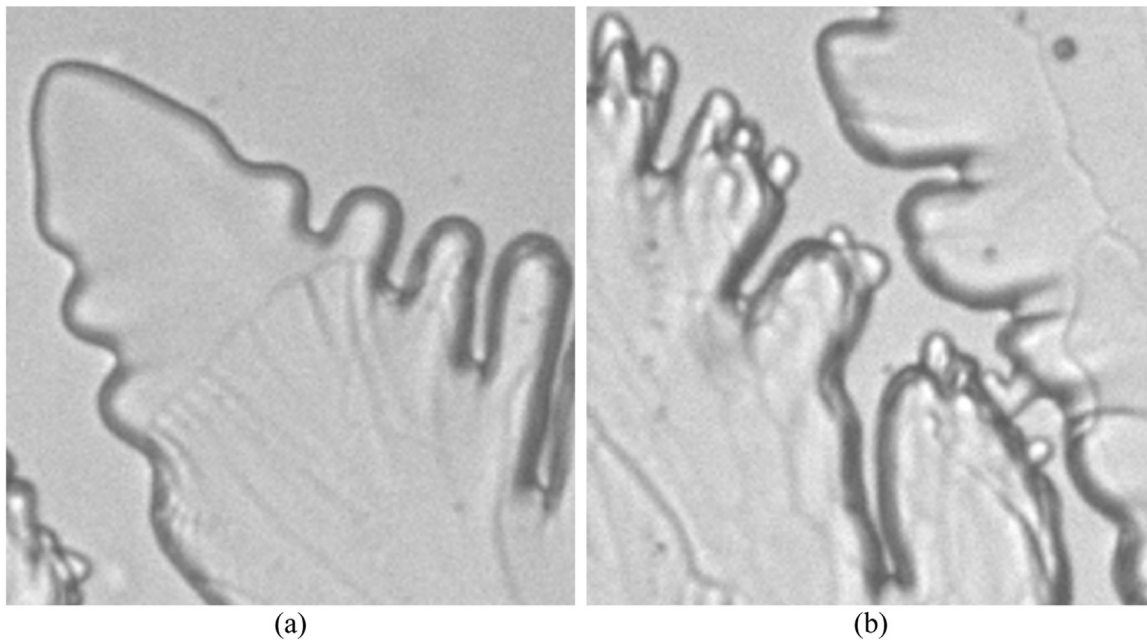


Fig. 3. : Magnified view taken from Fig. 2(b) showing the peritectic β -phase approaching a properitectic α -phase dendrite tip region (a) and β -phase bumps which immediately form at interfaces in interdendritic regions. After having been formed within $\Delta t=30$ s these bumps changed their morphology only sluggish. The width of the pictures is around 150 μm .

smaller bumps. These bumps may lead to bridging when the interdendritic distance is small (see Fig. 3(b)).

- After the β -phase has covered the α -dendrites, more and more polycrystalline-like objects appear at the elongated traces of the dense β -phase seaweed morphology (see Fig. 4).

For direction solidification the tip undercooling of dendrites or cells can be approximated [45] by

$$\Delta T = \Delta T_c + \Delta T_r = mc_0[1 - A(P_c)] + \frac{2\Gamma}{R} \tag{1a}$$

$$\text{with } A(P_c) = [1 - (1 - k)\Omega(P_c)]^{-1} \tag{1b}$$

where

$$\Omega(P_c) = \begin{cases} \text{Iv}(P_c) & \text{for parabolic dendrite tips} \\ P_c & \text{for hemispherical cell tips} \end{cases} \tag{2}$$

Assuming similar Gibbs-Thomson coefficients for both phases, namely the one from NPG ($\Gamma=7.6 \cdot 10^{-8}$ mK published in [48]), we get for the curvature undercoolings $\Delta T_r^\alpha = 0.008$ K and $\Delta T_r^\beta = 0.005$ K and for the solutal undercoolings $\Delta T_c^\alpha = 1.13$ K and $\Delta T_c^\beta = 0.17$ K. With $G = 6.65$ K/mm it becomes clear that after having overgrown the α -dendrites, the β -cells may further grow by another 144 μm to reach their steady cell tip position.

The α -dendrites with the experimentally determined primary arm spacing of more than 260 μm growing in a 100 μm gap between to glass plates are indeed closer to two dimensional objects than to a 3D dendrite. From Fig. 1(a) it is obvious that the dendrites revealed only two sidearm directions rather than four. However, the overgrowth of these flat α -dendrites by the β -phase happened simultaneously between (i) the flat α -dendrites and the tubing wall and (ii) in the interdendritic spacings between the dendrites. From that fact it can be concluded that the growth mechanism of the β -phase is equal whether

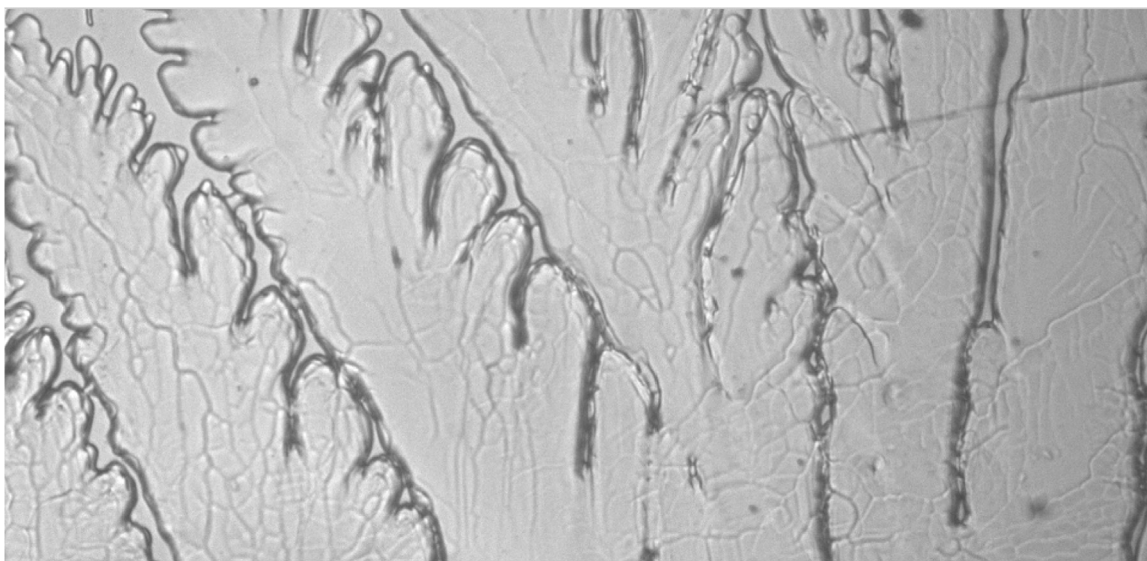


Fig. 4. : After rapid overgrowth of the α -phase dendrites with a compact β -phase seaweed structure, more and more polycrystalline-like objects appear at the elongated traces of the dense β -phase seaweed morphology.

it grew between α -dendrites and the wall or along α -dendrites in the interdendritic region.

Note that it might be argued that the β -growth between α -dendrites and tubing wall may be a pure solid-state transformation as no liquid might be present between the dendrites and the wall. This statement turns out to be wrong as without any liquid the mechanism for growth between α -dendrites and wall would be different compared to the growth between individual dendrites and this is not the case. Thus, we believe that between the α -dendrites and tubing walls there was still some remaining liquid.

Remarkable is the fact that the growth of β between the α -dendrites and the tubing walls reveals a very specific morphology. This morphology resembles the sidebranches of the “surface” dendrites presented in [47]. This author observed that while rapidly cooling a segment of a fine capillary filled with different dilute Succinonitrile-Argon alloys, solidification happens via thin solid layers propagating through the observation window. These surface dendrites revealed a dendritic growth pattern with close-spaced sidebranches of different morphologies. It was found that those surface dendrites revealed a doublet tip and three different classes of side branches: (A) cellular sidebranches, (B) dendritic sidebranches, and (C) an unsteady pattern, which were termed cauliflower structure - a specific type of what is nowadays called seaweed growth morphology. Note the similarity of the structure shown as Fig. 5(b) in [47] with that of the present Fig. 3(a). Note also that the morphology observed resembles also the thin (17 ± 2 nm) pure isotactic polystyrene films growing at larger melt undercoolings [49].

Seaweed growth was reported in solidification experiments on organic transparent alloys in thin samples [50–55], in which the preferred crystal growth direction had an angle to the thermal gradient. In [54] three different seaweed morphologies were distinguished: degenerate, stabilized, and strongly tilted seaweed. None of them are exactly like the morphology with which the β -phase covered the flat side of the α -dendrites. Degenerate seaweeds reveal tips that split alternately at regular intervals. This morphology occurs when a thin cubic crystal of transparent alloy grows close to the {111} plane [52–54]. Stabilized seaweeds do not show alternate tip splitting. This morphology was found to occur when a thin crystal of Succinonitrile alloy grows in the direction of non-negligible interface-energy anisotropy at a relatively large pulling velocity [54]. In these thin samples strongly tilted seaweed occurred when the growth direction is tilted by more than 45° to the pulling direction again at even larger pulling velocity. As stated in [56], seaweeds are believed to be allied by nature to the low anisotropy of the solid/liquid interface energy because growth is then not constrained to some specific orientation.

In the case of a thin solid layer solidifying with closed contact along a substrate (glass or a second solid phase), growth may be affected by the substrate/solid/liquid three junction line which might reduce the effect of the anisotropy of solid/liquid surface tension leading to a less anisotropic “effective” surface tension.

Fast growth of compact seaweed structures were numerically predicted in 1992 by Shochet et al. [57]. More recently, several authors have simulated the occurrence of seaweed growth morphologies using the phase field method [56,58–60]. The morphology which comes the closest to the one we are reporting is the one which is called compact seaweed by Amoozazei et al. [58]. They have studied alloys when anisotropies in the processing environment compete with the inherently anisotropic properties of the growing material, and found in their 2D simulations the occurrence of compact seaweed for higher interface velocity and lower temperature gradients.

Next, we would like to discuss the appearance of the bumps of β -phase in the interdendritic region (Fig. 3(b)). From the observation it became obvious, that β covers the α -dendrites from all sides, namely between the flat side and the tubing wall as well as in the interdendritic region. As mentioned above the growth rate of the newly formed β -layer is 10 times faster than the pulling rate. From the observations no clear statement can be made about its thickness. However, the

formation of the bumps reveal the fact that the amount of β that has formed is not in equilibrium with the supersaturated interdendritic liquid. Obviously, the rapid growth of the thin β -layer as compact seaweed is governed only partly by the supersaturated interdendritic liquid. To a larger extent it is governed by the contact between the two solid phases via the moving three phase junction line (α/β /liquid) and the large tip curvature perpendicular to the α -dendrite. Thus, the surface of the thin β -layer is not equilibrated with the interdendritic liquid and so it gets morphologically unstable and those cellular bumps form (at least in growth direction). However, the hereby rejected solute rapidly increases the interdendritic solute content and so β equilibrates with the interdendritic liquid and the growth of the bumps stops. Further growth is orders of magnitude slower and caused by the overall sample pulling.

The last point to be discussed is the observation that after the β -phase has covered the α -dendrites, more and more polycrystalline-like objects appear at the elongated traces of the dense β -phase seaweed morphology (see Fig. 4). Unfortunately, no “post mortem” metallographic examination of crystal orientation by e.g. EBSD is possible with such an organic compound. Thus, the crystal orientation of the newly formed polycrystalline-like objects remains unknown. However, the whole process resembles the recrystallization process after generation of a massive amount of lattice defects by e.g. rolling [61–63]. It is conceivable that during the rapid growth of the β -compact seaweed, lots of crystal defects are incorporated, and as the diffusion distances are small, nucleation and growth of differently orientated new grains may help to relax the microstructure. However, this statement must be seen as purely hypothetical.

4. Conclusion

During a 16 h directional solidification experiment with a TRIS-NPG alloy with a concentration which corresponds to the hyperperitectic limit, we have observed a transition from α -dendritic to β -cellular growth. This transition happened with the same speed (i) between the α -dendrites and the tubing wall and (ii) between individual α -dendrites. In the liquid between the α -dendrites and the tubing wall, the thin solid β -phase grew with a compact seaweed morphology. This finding may reveal the generic nature of this compact seaweed structure as morphology a thin solid layer may take when growing on a substrate. In the interdendritic regions between the α -dendrites, the β -phase produced rapidly cellular-like bumps in growth direction until the β -phase and the interdendritic solute content is in equilibrium. Some distance behind the overgrowth scenario, more and more polycrystalline-like objects form at the elongated traces of the dense β -phase seaweed morphology, which might be a recrystallization process happening to relax the rapidly formed thin β -phase microstructure.

Acknowledgment

This work was supported in part by the European Space Agency ESA (ESTEC Contract No. 14243/00/NL/SH) through means of the ESA map project METCOMP and in part by the Austrian Space Agency ASA within the frame of the METTRANS-ISS project.

References

- [1] J.A. Dantzig, M. Rappaz, *Solidification*, EPFL Press, Lausanne, Switzerland, 2009.
- [2] D.R. Uhlmann, G.A. Chadwick, Unidirectional solidification of melts producing the peritectic reaction, *Acta Met.* 9 (1961) 835–840.
- [3] W.J. Boettinger, The structure of directionally solidified two-phase Sc-Cd peritectic alloys, *Met. Trans.* 5 (1974) 2023–2031.
- [4] H. Yasuda, N. Notake, K. Tokieda, I. Ohnaka, Periodic structure during unidirectional solidification for peritectic Cd-Sn alloys, *J. Cryst. Growth* 210 (2000) 637–645.
- [5] R. Trivedi, J.S. Park, Dynamics of microstructure formation in the two-phase region of peritectic systems, *J. Cryst. Growth* 235 (2002) 572–588.

- [6] R. Trivedi, J.H. Shin, Modelling of microstructure evolution in peritectic systems, *Mater. Sci. Eng. A* 414 (2005) 288–295.
- [7] F. Kohler, L. Germond, J.D. Wagnière, M. Rappaz, Peritectic solidification of Cu-Sn alloys: microstructural competition at low speed, *Acta Mater.* 57 (2000) 56–68.
- [8] A. Karma, W.J. Rappel, B.C. Fuh, R. Trivedi, Model of banding in diffusive and convective regimes during directional solidification of peritectic systems, *Met. Mater. Trans. A* 29 (1998) 1457–1470.
- [9] K. Tokieda, H. Yasuda, I. Ohnaka, Formation of banded structure in Pb-Bi peritectic alloys, *Mater. Sci. Eng. A* 262 (1999) 238–245.
- [10] T.A. Lograsso, B.C. Fuh, R. Trivedi, Phase selection during directional solidification of peritectic alloys, *Met. Mater. Trans. A* 36 (2005) 1287–1300.
- [11] S. Liu, R. Trivedi, Effect of thermosolutal convection on microstructure formation in the Pb-Bi peritectic system, *Met. Trans. A* 37 (2006) 3293–3304.
- [12] X.W. Hu, S.M. Li, W.J. Chen, S.F. Gao, L. Liu, H.Z. Fu, Primary dendrite arm spacing during unidirectional solidification of Pb – Bi peritectic alloys, *J. Alloy. Compd.* 484 (2009) 631–636.
- [13] Y. Li, S.C. Ng, H. Jones, Observation of lamellar eutectic-like structure in a Zn-rich Zn-3.37wt%Cu peritectic alloy processed by Bridgman solidification, *Scr. Mater.* 39 (1998) 7–11.
- [14] D. Ma, Y. Li, S.C. Ng, H. Jones, Unidirectional solidification of Zn-rich Zn-Cu peritectic alloys - II. Microstructural length scales, *Acta Mater.* 48 (2000) 1741–1751.
- [15] D. Ma, Y. Li, S.C. Ng, H. Jones, Unidirectional solidification of Zn-rich Zn-Cu peritectic alloys-I Microstructure selection, *Acta Mater.* 48 (2000) 419–431.
- [16] A.P. Titchener, J.A. Spittle, The microstructures of directionally solidified alloys that undergo a peritectic transformation, *Acta Mater.* 23 (1975) 497–502.
- [17] X.W. Hu, S.M. Li, L. Liu, H.Z. Fu, Microstructures evolution of directionally solidified Sn-16%Sb hyperperitectic alloy, *China Foundry* 5 (2008) 167–171.
- [18] P. Busse, F. Meissen, Coupled growth of the properitectic α - and the peritectic γ -phases in binary titanium aluminides, *Scr. Mater.* 37 (1997) 653–658.
- [19] Y.Q. Su, C. Liu, X.Z. Li, J.J. Guo, B.S. Li, J. Jia, H.Z. Fu, Microstructure selection during the directionally peritectic solidification of Ti-Al binary system, *Intermetallics* 13 (2005) 267–274.
- [20] W. Luo, J. Shen, Z. Min, H. Fu, Lamellar orientation control of TiAl alloys under high temperature gradient with a Ti-43Al-3Si seed, *J. Cryst. Growth* 24 (2008) 5441–5446.
- [21] M. Vandyoussefi, H.W. Kerr, W. Kurz, Directional solidification and δ/γ solid state transformation in Fe3% Ni alloy, *Acta Mater.* 45 (1997) 4093–4105.
- [22] M. Vandyoussefi, H.W. Kerr, W. Kurz, Two-phase growth in peritectic Fe-Ni alloys, *Acta Mater.* 48 (2000) 2297–2306.
- [23] M. Sumida, Evolution of two phase microstructure in peritectic Fe-Ni alloy, *J. Alloy. Compd.* 349 (2003) 302–310.
- [24] T.S. Lo, S. Dobler, M. Plapp, A. Karma, W. Kurz, Two-phase microstructure selection in peritectic solidification: from island banding to coupled growth, *Acta Mater.* 51 (2003) 599–611.
- [25] S. Dobler, T.S. Lo, M. Plapp, A. Karma, W. Kurz, Peritectic coupled growth, *Acta Mater.* 52 (2004) 2795–2808.
- [26] Y.Q. Su, L.S. Luo, X.Z. Li, J.J. Guo, H.M. Yang, H.Z. Fu, Well-aligned in situ composites in directionally solidified Fe-Ni peritectic system, *Appl. Phys. Lett.* 89 (2006) 2319181–2319183.
- [27] L.S. Luo, Y.Q. Su, J.J. Guo, X.Z. Li, H.Z. Fu, A simple model for lamellar peritectic coupled growth with peritectic reaction, *Sci. China Phys. Mech. Astron.* 50 (2007) 442–450.
- [28] L.S. Luo, Y.Q. Su, J.J. Guo, X.Z. Li, S.M. Li, H. Zhong, L. Liu, H.Z. Fu, Peritectic reaction and its influences on the microstructures evolution during directional solidification of Fe-Ni alloys, *J. Alloy. Compd.* 461 (2008) 121–127.
- [29] L.S. Luo, Y.Q. Su, X.Z. Li, J.J. Guo, H.M. Yang, H.Z. Fu, Producing well aligned in situ composites in peritectic systems by directional solidification, *Appl. Phys. Lett.* 92 (2008) 61903.
- [30] Z.R. Feng, J. Shen, Z.X. Min, L.S. Wang, H.Z. Fu, Two phases separate growth in directionally solidified Fe-4.2Ni alloy, *Mater. Lett.* 64 (2010) 1813–1815.
- [31] J.H. Lee, J.D. Verhoeven, Peritectic formation in the Ni-Al system, *J. Cryst. Growth* 144 (1994) 353–366.
- [32] Q.L. Rao, X.L. Fan, D. Shu, C.C. Wu, In-situ XRD study on the peritectic reaction of YBCO thin film on MgO substrate, *J. Alloy. Compd.* 461 (2008) L29–L33.
- [33] H. Zhong, S.M. Li, H.Y. Lü, L. Liu, G.R. Zou, H.Z. Fu, Microstructure evolution of peritectic Nd14Fe79B7 alloy during directional solidification, *J. Cryst. Growth* 310 (2008) 3366–3371.
- [34] A. Ludwig, J. Mogeritsch, M. Grasser, In-situ observation of unsteady peritectic growth modes, *Trans. Indian Inst. Met.* 62 (2009) 433–436.
- [35] J. Mogeritsch, A. Ludwig, S. Eck, M. Grasser, B.J. McKay, Thermal stability of a binary non-faceted/non-faceted peritectic organic alloy at elevated temperatures, *Scr. Mater.* 60 (2009) 882–885.
- [36] J. Mogeritsch, S. Eck, M. Grasser, A. Ludwig, In situ observation of solidification in an organic peritectic alloy system, *Mater. Sci. Forum* 649 (2010) 159–164.
- [37] A. Ludwig, J. Mogeritsch, In-situ observation of coupled peritectic growth, in: *Proceedings of the Solidif. Sci. Technol. John Hunt International. Symp.*, 2011, pp. 233–242.
- [38] J. Mogeritsch, A. Ludwig, In-situ observation of coupled growth morphologies in organic peritectics, *IOP Conf. Ser. Mater. Sci. Eng.* 27 (2011) 12028.
- [39] J. Mogeritsch, A. Ludwig, Microstructure formation in the two phase region of the binary peritectic organic system TRIS-NPG, in: *Proceedings of the TMS Annu. Meet. Symp. "Materials Res. Microgravity," Orlando, FL, 2012*, pp. 48–56.
- [40] A. Ludwig, J. Mogeritsch, Recurring instability of cellular growth in a near peritectic transparent NPG-TRIS alloy system, *Mater. Sci. Forum* 790–791 (2014) 317–322.
- [41] J. Mogeritsch, A. Ludwig, In-situ observation of the dynamic of peritectic coupled growth using the binary organic system TRIS-NPG, *IOP Conf. Ser. Mater. Sci. Eng.* 84 (2015) 12055.
- [42] M. Barrio, D.O. Lopez, J.L. Tamarit, P. Negrier, Y. Haget, Degree of Miscibility between Non-isomorphous Plastic Phases: Binary system NPG (neopentyl glycol)-TRIS [tris(hydroxymethyl)aminom], *J. Mater. Chem.* 5 (1995) 431–439.
- [43] J. Mogeritsch, Investigation on peritectic solidification using a transparent organic system P.H.D. Thesis, Montanuniversität Leoben, AUT, 2012.
- [44] A. Ludwig, J. Mogeritsch, M. Kolbe, G. Zimmermann, L. Sturz, N. Bergeon, B. Billia, G. Faivre, S. Akamatsu, S. Bottin-Rousseau, D. Voss, Advanced solidification studies on transparent alloy systems: a new european solidification insert for Material Science Glovebox on board the International Space Station, *JOM* 64 (2012) 1097–1101.
- [45] W. Kurz, D.J. Fisher, *Fundamental of Solidification*, 4th ed., Trans. Tech. Publ., Aedermansdorf, 1998.
- [46] S. Gurevich, A. Karma, M. Plapp, R. Trivedi, Phase-field study of three-dimensional steady-state growth shapes in directional solidification, *Phys. Rev. E* 81 (2010) 11603.
- [47] A. Ludwig, Dendritic and cellular doublets: morphologies of thin solid films growing along a substrate during the initial state of solidification of bulk melts, *Phys. Rev. E* 59 (1999) 1893–1897.
- [48] Y. Ocak, S. Akbulut, K. Keslioglu, N. Marasli, Solid-liquid interfacial energy of Neopentylglycol, *Colloid Interface Sci.* 329 (2008) 555–562.
- [49] L. Granasy, T. Pusztai, T. Börzsönyi, J.A. Warren, J.F. Douglas, A general mechanism of polycrystalline growth, *Nat. Mater.* 3 (2004) 645–650.
- [50] T. Ihle, H. Müller-Krumbhaar, Diffusion-limited fractal growth morphology in thermodynamical two-phase systems, *Phys. Rev. Lett.* 70 (1993) 3083–3086.
- [51] T. Ihle, H. Müller-Krumbhaar, Fractal and compact growth morphologies in phase transitions with diffusion transport, *Phys. Rev. E* 49 (1994) 2972–2991.
- [52] S. Akamatsu, G. Faivre, T. Ihle, Symmetry-broken double fingers and seaweed pattern in thin-film directional solidification of nonfacted cubic crystal, *Phys. Rev. E* 51 (1995) 4751–4773.
- [53] B. Utter, R. Ragnarsson, E. Bodenschatz, Alternating tip splitting in directional solidification, *Phys. Rev. Lett.* 86 (2001) 4604–4607.
- [54] B. Utter, E. Bodenschatz, Dynamics of low anisotropy morphologies in directional solidification, *Phys. Rev. E* 66 (2002) 51604.
- [55] T. Guo, H. Li, G.X. Wang, Development of irregular interface morphology during unidirectional solidification of Succinonitrile, in: *Proceedings of the ASME Summer Heat Transf. Conference., Las Vegas, Nevada, 2003*, pp. 1–8.
- [56] Y. Chen, B. Billia, D.Z. Li, H. Nguyen-Thi, N.M. Xiao, A.-A. Bogno, Tip-splitting instability and transition to seaweed growth during alloy solidification in anisotropically preferred growth direction, *Acta Mater.* 66 (2014) 219–231.
- [57] O. Shochet, K. Kassner, B.-J. Eshel, S.G. Lipson, H. Müller-Krumbhaar, Morphology transitions during non-equilibrium growth, *Physica A* (1992).
- [58] M. Amoozrezaei, S. Gurevich, N. Provatas, Orientation selection in solidification patterning, *Acta Mater.* 60 (2012) 657–663.
- [59] J. Friedli, P. Di Napoli, M. Rappaz, J.A. Dantzig, Phase-field modeling of the dendrite orientation transition in Al-Zn alloys, *IOP Conf. Ser. Mater. Sci. Eng.* 33 (2012) 12111.
- [60] J.A. Dantzig, P. Di Napoli, J. Friedli, M. Rappaz, Dendritic growth morphologies in Al-Zn alloys—Part II: Phase-field computations, *Met. Mater. Trans. A* 44 (2013) 5532–5543.
- [61] P.B. Prangnell, J.S. Hayes, J.R. Bowen, P.J. Apps, P.S. Bate, Continuous recrystallisation of lamellar deformation structures produced by severe deformation, *Acta Mater.* 52 (2004) 3193–3206.
- [62] M. Crumbach, M. Goerdeler, G. Gottstein, Modelling of recrystallisation textures in aluminium alloys: I. Model set-up and integration, *Acta Mater.* 54 (2006) 3275–3289.
- [63] M. Crumbach, M. Goerdeler, G. Gottstein, Modelling of recrystallisation textures in aluminium alloys: II. Model performance and experimental validation, *Acta Mater.* 54 (2006) 3291–3306.